Institut für Energietechnik und Thermodynamik

Forschungsbereich Strömungsmaschinen

Research Objective

Especially when operating in pump-mode, part load flow in pump-turbines is still a challenging task since crucial flow regimes become apparent in the entire flow domain. In deep part load, the occurrence of flow instabilities is evident. Flow phenomena like rotating stall in the guide vane or pre-rotating flow at the runner inlet are mainly responsible for an improper blade load. Another consequence is oscillating flow upstream of the runner, which results in the so called "off-design" operating conditions , see Fig.1-left.

Existing modeling approaches and further developments of linear eddy-viscosity RANS models considering rotation effects are implemented into the CFD software and validated by means of generic flow problems. The two-equation turbulence model SST k-ω is primarily employed for sensitizing methods used for transient incompressible single- and two-phase flow simulation. Simulation results of pump-turbine flow are directly compared with experiments making the interpretation of results more reliable.

A practical two-phase study considers the performance break-up due to leading edge cavitation of the pump-turbine runner during low partial flow rates, as well as a direct comparison with test-rig measurements.

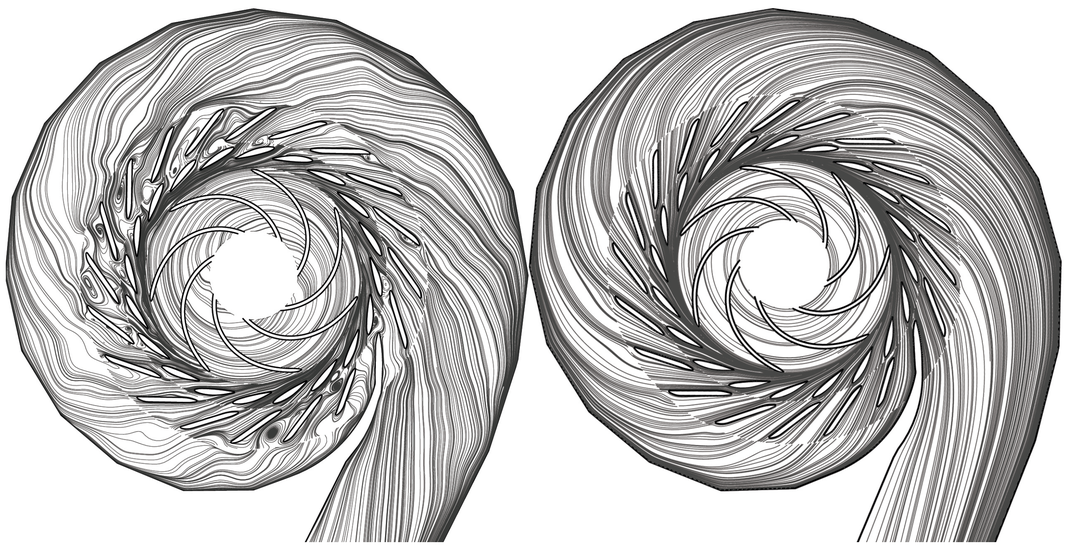

Fig.1 :Instantaneous streamlines of C at $r_z = 0$ - Right: $Q/Q_N = 0.4$; Left: $Q/Q_N = 1$.

Implementation and Validation

The correction method implemented was suggested by Smirnov et al. and applied to the standard SST k-ω, suggested by Menter. The correction goes linearly into the transport equation for both k and ω via $\mathcal{P}_{\text{corr}} = \mathcal{P} f_{\text{r1}}$ using the relationship

$$f_{\text{r1}} = (1 + c_{r1}) \frac{2r^*}{1 + r^*} \left(1 - c_{r3} \tan^{-1}(c_{r2} \widetilde{r}\right) - c_{r1}), \tag{1}$$

with $c_{r1} = 1.0$, $c_{r2} = 2.0$ and $c_{r3} = 1.0$. The empirical function f_{r1} depends on the scalar quantities $\tilde{r}$ and $\bar{r}$, which basically characterize the ratio between strain and vorticity of the flow:

$$r^* = \frac{|\mathbf{S}|}{|\mathbf{W}_{\text{eff}}|} \qquad \widetilde{r} = \frac{2 W_{ik,\text{eff}} S_{jk}}{|\mathbf{W}_{\text{eff}}| D^3} \left(\frac{D S_{ij}}{Dt} + (\epsilon_{imn} S_{jn} + \epsilon_{jmn} S_{in}) \Omega^m \right) \tag{2}$$

ϵ stands for the Levi-Civita symbol and $D = max(|\mathbf{S}|^2, \beta^* \omega^2)$. The material derivation of the strain-rate tensor $\mathbf{S}$ has to be computed from

$$\dot{S}_{ij} = \frac{\partial S_{ij}}{\partial t} + C_i \frac{\partial S_{ij}}{\partial x_j}. \tag{3}$$

No further solver setting has to defined, as both derivatives are computed explicitly from the mean velocity field.

Figure 3-right shows the velocity distributions across the channel for the sensitized SST-CC k-ω model and the turbulent kinetic energy. The curve of k at $Ro = 0.5$ clearly shows the typical asymmetric distribution due to rotation. On the pressure side, the turbulence production is accelerated whereas on the suction side the turbulent energy peak vanishes at an increasing rotation level. In a diffuser with swirl inflow, the correction leads to an improvement in the peak value of the azimuthal velocity $C_\theta(r)$ as well as a better linearity of the curve towards diffuser centerline, as can be seen from Fig.3-left.

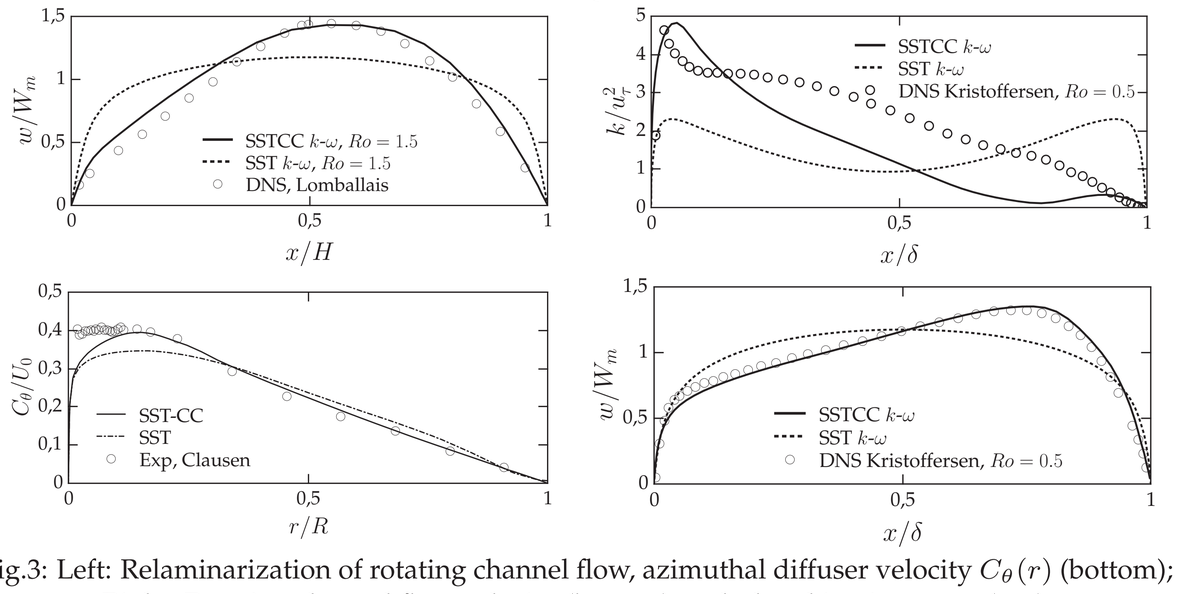

Fig.3: Left: Relaminarization of rotating channel flow, azimuthal diffuser velocity $C_\theta(r)$ (bottom); Right: Rotating channel flow velocity (bottom), turbulent kinetic energy (top).

Part Load Flow of a Pump-turbine

Table 1 shows the comparison between experiments and global flow quantities using the standard SST k-ω and the modified SST-CC k-ω model including the corresponding relative error, denoted as Δ. The corresponding dimensionless factors are given by

$$Q_{nD} = \frac{Q}{n D_{\text{ref}}^3} \qquad T_{nD} = \frac{T_m}{\rho n^2 D_{\text{ref}}^5} \tag{4}$$

Discharge Factor Torque Factor

Table 1 lists two exemplary operation points ($Q/Q_N = 0.4$ and $Q/Q_N = 0.2$) in pump mode. When using the corrected model, the global quantities show a better agreement with the measurement data than the uncorrected one in both operating points.

Q/Q_N	data type	T	H	n_{ED}	E_{nD}	T_{nD}	Δn_{ED}	ΔE_{nD}	ΔT_{nD}
-		Nm	m	-	-	-	%	%	%
0.4	EXP	388.00	22.56	-0.248	16.292	1.348			
	SST k-ω	403.51	24.25	-0.239	17.516	1.407	3.56	-7.51	-4.384
	SST-CC k-ω	378.57	23.65	-0.242	17.080	1.320	2.33	-4.83	2.066
0.2	EXP	276.30	24.08	-0.240	17.392	0.960			
	SST k-ω	292.85	25.25	-0.234	18.233	1.021	2.336	-4.840	-6.385
	SST-CC k-ω	273.92	25.02	-0.235	18.071	0.955	1.898	-3.908	0.493

Tab.1: Comparison of global quantities.

Figure 2 shows velocity components of the pump-turbine mean flow compared to experiments from Edinger. As can be seen from Fig.2-left, typical prerotating flow with a strong recirculation zone occurs during deep part load operation. The right velocity represent the circumferential velocity component of the stay vane channel flow.

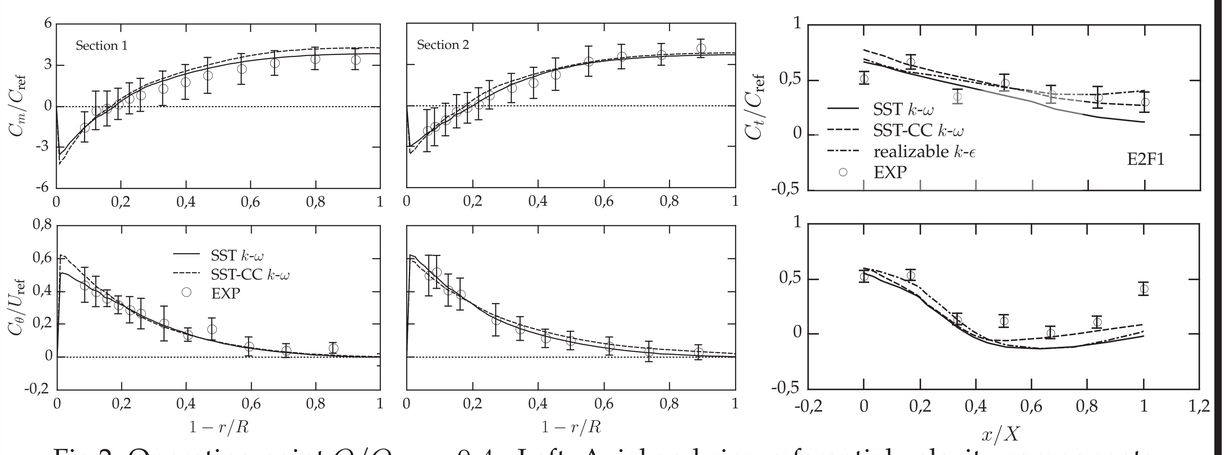

Fig.2: Operating point $Q/Q_N = 0.4$ - Left: Axial and circumferential velocity components; Right: secondary flow in the stay vane channel.

Cavitating Flow

The cavitating flow test case (Rouse & Macnown) considers a hemispherical body in a free flow at Re $= 1.3 \times 10^5$ and $AoA = 0°$, for which a 3D computational mesh with 8.5×10^5 cells is used and standard boundary conditions are defined. Figure 4-right shows a typical ring-shaped cavity starting straight after the curved head form of the cylinder. In Fig.4-left, the C_p-curves are in good agreement with the measured data, although the results show a slight overestimation of the low-pressure field size at the cylinder wall.

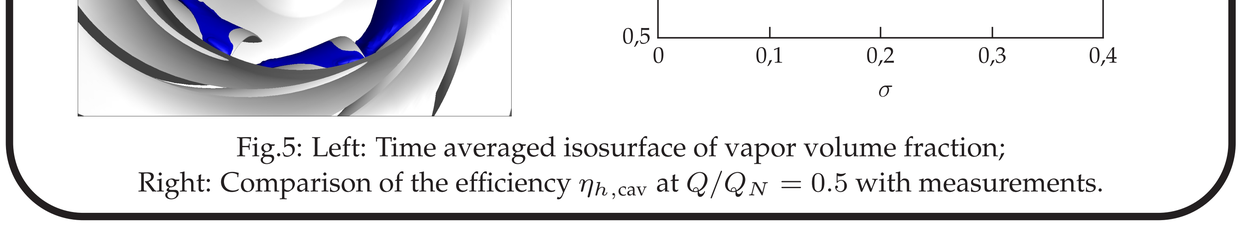

Fig.4: Left: time averaged dimensionless pressure C_p at different σ-values; Right: iso-surface of the circular cavity sheet at $\sigma = 0.4$.

Fully resolved cavitation in rotating machineries based on two phase flow, requires extensive computational resources and numerical stability as well, due to the rotating mesh domain. Since no standard two-phase solver contain mass transfer models in dynamic meshes in OpenFOAM, the restructuring of a new solver has to be done on the basis of other existing solvers.

Fig.5: Left: Time averaged isosurface of vapor volume fraction; Right: Comparison of the efficiency $\eta_{h,\text{cav}}$ at $Q/Q_N = 0.5$ with measurements.